Environmental Science & Technology

Article

pubs.acs.org/est

Derivation of Hydroperoxyl Radical Levels at an Urban Site via Measurement of Pernitric Acid by Iodide Chemical Ionization Mass Spectrometry

Dexian Chen,[†,#] L. Gregory Huey,[*,†] David J. Tanner,[†] Jianfeng Li,[†] Nga L. Ng,[†,‡] and Yuhang Wang[†]

[†]School of Earth and Atmospheric Sciences, Georgia Institute of Technology, 311 Ferst Drive, Atlanta, Georgia 30332, United States

[‡]School of Chemical and Biochemical Engineering, Georgia Institute of Technology, Atlanta, Georgia 30332, United States

Supporting Information

ABSTRACT: Hydroperoxyl radical (HO_2) is a key species to atmospheric chemistry. At warm temperatures, the HO_2 and NO_2 come to a rapid steady state with pernitric acid (HO_2NO_2). This paper presents the derivation of HO_2 from observations of HO_2NO_2 and NO_2 in metropolitan Atlanta, US, in winter 2014 and summer 2015. HO_2 was observed to have a diurnal cycle with morning concentrations suppressed by high NO from the traffic. At night, derived HO_2 levels were nonzero and exhibited correlations with O_3 and NO_3, consistent with previous studies that ozonolysis and oxidation by NO_3 are sources of nighttime HO_2. Measured and model calculated HO_2 were in reasonable agreement: Without the constraint of measured HO_2NO_2, the model reproduced HO_2 with a model-to-observed ratio (M/O) of 1.27 (r = 0.54) for winter, 2014, and 0.70 (r = 0.80) for summer, 2015. Adding measured HO_2NO_2 as a constraint, the model predicted HO_2 with M/O = 1.13 (r = 0.77) for winter 2014 and 0.90 (r = 0.97) for summer 2015. These results demonstrate the feasibility of deriving HO_2 from HO_2NO_2 measurements in warm regions where HO_2NO_2 has a short lifetime.

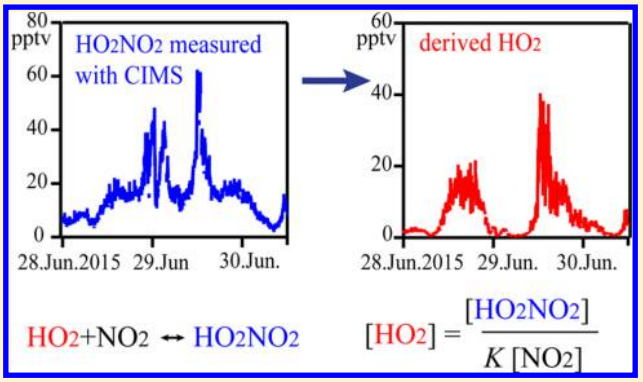

INTRODUCTION

Hydroperoxyl radical (HO_2) plays a key role in the atmosphere and is the dominant form of HO_x (OH + HO_2). Sources of HO_2 include the oxidation of CO and volatile organic compounds (VOC) by hydroxyl radicals (OH), the photolysis of carbonyl compounds, the ozonolysis of alkenes, and the oxidation of VOC by the nitrate radical (NO_3).[1−6] The last two are important sources of HO_2 at night. HO_2 is involved in many important atmospheric processes such as the degradation of pollutants, ozone production, and secondary organic aerosol (SOA) formation.[7−9] Observations of HO_2 are important for understanding and constraining atmospheric chemistry.

Pernitric acid (HO_2NO_2) is closely coupled to HO_2 levels in many regions of the atmosphere. HO_2NO_2 has a relatively simple chemistry in the atmosphere (Reactions 1−4).[10−14]

$$HO_2 + NO_2 + M \rightleftarrows HO_2NO_2 + M \quad (1)$$

$$HO_2NO_2 + h\nu \rightarrow HO_2 + NO_2 \quad (2a)$$

$$\rightarrow OH + NO_3 \quad (2b)$$

$$HO_2NO_2 + OH \rightarrow NO_2 + O_2 + H_2O \quad (3)$$

$$HO_2NO_2 \rightarrow \text{deposition/scavenging} \quad (4)$$

The thermal decomposition rate k_{-1} is a strong function of temperature, e.g., ∼5 × 10^{-6} s^{-1} at −30 °C and ∼1 × 10^{-1} s^{-1} at 30 °C.[15] The important role of HO_2NO_2 in HO_x and NO_x ($NO + NO_2$) chemistry in cold regions has been widely discussed.[14,16−23] In warm regions, as its thermal decomposition is fast and dominates the loss, HO_2NO_2 chemistry is reduced to a rapidly established steady state with HO_2 and NO_2 (Reaction 1). Given proper averaging time that allows the equilibrium to be approached, HO_2 can be derived from HO_2NO_2 and NO_2 observations.[24]

$$[HO_2] = \frac{k_{-1}[HO_2NO_2]}{k_1[NO_2]} = \frac{[HO_2NO_2]}{K[NO_2]} \quad (5)$$

where $K = k_1/k_{-1}$ is the equilibrium constant and K is a function of temperature alone.[15]

In this work, we employ chemical ionization mass spectrometry (CIMS) to measure HO_2NO_2 in metropolitan Atlanta and determine HO_2 from observations of HO_2NO_2 and NO_2. Hydrated iodide ($I^-\cdot(H_2O)_n$) is used as the reagent ion(s) for CIMS detection of HO_2NO_2.[25−27] The $I^-\cdot(H_2O)_n$ CIMS

Received: October 17, 2016
Revised: February 6, 2017
Accepted: February 17, 2017
Published: February 17, 2017

DOI: 10.1021/acs.est.6b05169
Environ. Sci. Technol. 2017, 51, 3355−3363

Table 1. Summary of the Measurements in Two Seasons

	species	technique	LOD	integration Time	uncertainty
winter (2014)	HO_2NO_2	CIMS	0.2 pptv	1 min	±22%
	N_2O_5	CIMS[33]	0.2 pptv	1 min	±25%
	NO	chemiluminescence[69]	4.5 pptv	1 min	±10%
	NO_2	CAPS[47]	<60 pptv	5 s	<5%
	O_3	Thermo 49C	<1 ppbv	10 s	±1 ppbv
	CO	Thermo 48C	<1 ppbv	10 s	±5%
	met. parameters[a]	Vantage Pro2		1 min	
summer (2015)	HO_2NO_2	CIMS[27]	0.6 pptv	1 min	±16%
	NO	Teledyne 200EU	50 pptv	1 min	±5%
	NO_2	CAPS[33]	<60 pptv	5 s	<5%
	O_3	Teledyne T400	400 pptv	10 s	±5%
	CO	IR adsorption cell	<1 ppbv	10 s	±5%
	met. parameters[a]	Vantage Pro2		1 min	

[a]Meteorological parameters include T, p, humidity, wind speed, wind gust, wind direction, total solar radiation, solar UV radiation, cloud base, and precipitation rate.

technique is versatile and suitable for detections of a host of species, such as Cl_2, Br_2, ClO, BrO, HOCl, HOBr, N_2O_5, HNO_3, HONO, $ClNO_2$, HCOOH, HNCO, and $CH_3C(O)OOH$.[28−39] Consequently, HO_2NO_2 observations and determination of HO_2 can be simultaneously performed with measurements of other species using the same instrument. The goal of this work is to evaluate the feasibility of deriving HO_2 from HO_2NO_2 observations in a warm polluted environment. This work on deriving HO_2 from HO_2NO_2 observations utlizing $I^-\cdot(H_2O)_n$ as a reagent ion was also motivated as we have found that we cannot directly measure HO_2 with $I^-\cdot(H_2O)_n$ without significant interferences as detailed by Sanchez et al.[40]

EXPERIMENTAL METHODS

Observations. Observations were made in both winter (November 20, 2014 to January 2, 2015) and summer (June 10 to 7 July, 2015), on top of the Georgia Tech Ford ES&T building in metropolitan Atlanta (33°46′ N, 84°24′ W), 10 m above the ground, and 0.6 km to the west of the Interstate-75/85 highway. Concurrent measurements of HO_2NO_2, NO, NO_2, CO, O_3, and N_2O_5 (winter only) and meteorological parameters were performed (Table 1). All instruments for gas phase species were housed in a laboratory on the top floor with inlets extending through the roof to sample ambient air. Basic meteorological parameters were measured by a weather station mounted on the roof of the building. Data were reported in local time, UTC−5 h in winter, and UTC−4 h in summer.

CIMS Measurements of HO_2NO_2. The general CIMS instrumentation and methodology have been discussed by Huey.[41] Due to instrument availability, we employed different CIMS instruments for each season. Both CIMS instruments had configurations similar to that described by Liao et al.[29] The main differences were inlet configurations and flows. The inlets were Teflon FEP tubing (O.D. = 1.22 cm and I. D. = 0.95 cm), 9 and 5 m long, respectively, in winter and summer observations. The inlet flows were 46 slpm (standard liter per minute, standard = 0 °C and 1013 hPa) and 41 slpm, respectively, of which roughly 1.5 slpm was sampled into CIMS and the rest was exhausted. These large flows resulted in relatively short residence times in the inlets, roughly 0.8 and 0.5 s, respectively. We also assessed the inlet loss of HO_2NO_2 under the same conditions (i.e., flow rate and temperature) as the ambient measurement. HO_2NO_2 was synthesized (Supporting Information), diluted, and flown through (1) the inlet used for sampling, (2) a new, clean inlet of the same diameter and length as the sampling inlet, and (3) a very short (∼30 cm), clean inlet of the same diameter. HO_2NO_2 signals were found to be the same for all cases, and thus, we concluded that the wall loss of HO_2NO_2 was minimal.

The detection of HO_2NO_2 using $I^-\cdot(H_2O)_n$ CIMS was similar to that described by Veres et al.[27] Briefly, HO_2NO_2 is ionized by $I^-\cdot(H_2O)_n$ and detected on two channels: $HO_2NO_2\cdot I^-$ and NO_3^-.

$$I^-\cdot(H_2O)_n + HO_2NO_2 \rightarrow HO_2NO_2\cdot I^-(m/z\,206) + nH_2O \quad (6)$$

$$I^- + HO_2NO_2 \rightarrow NO_3^-(m/z\,62) + HOI \quad (7a)$$

$$I^-\cdot(H_2O)_n + HO_2NO_2 \rightarrow NO_3^-(m/z\,62) + HOI + nH_2O \quad (7b)$$

We retrieved HO_2NO_2 concentrations based on the $HO_2NO_2\cdot I^-$ channel. We found that the NO_3^- channel is the major channel with a branching ratio >90%. However, it is known to be nonspecific for HO_2NO_2. It can be formed via reactions of $I^-\cdot(H_2O)_n$ and several other species (N_2O_5, NO_3, $BrONO_2$, $ClONO_2$).[37,41−43] An assessment of the NO_3^- channel is given in the Supporting Information.

As we used a quadrupole mass spectrometer of unit mass resolution, the detection at the $HO_2NO_2\cdot I^-$ channel can be interfered with by $I\cdot{}^{79}Br^-$ of the same m/z in a bromine-rich environment.[30]

$$HOBr + I^-\cdot(H_2O)_n \rightarrow I\cdot Br^-(m/z\,206,\ 208) + \ldots \quad (8)$$

Since the sensitivities to isotopes are proportional to their abundances, this interference can be corrected by tracking the isotope $I\cdot{}^{81}Br^-$ at m/z 208. Nitryl chloride ($ClNO_2$) is detected as $ClNO_2\cdot I^-$ at m/z 208 ($^{35}ClNO_2\cdot I^-$) and 210 ($^{37}ClNO_2\cdot I^-$).[33] If $ClNO_2$ is present, the $^{35}ClNO_2\cdot I^-$ signal at m/z 208 needs to be subtracted to obtain the $I\cdot{}^{81}Br^-$ signal, and thus, the $^{37}ClNO_2\cdot I^-$ signal at m/z 210 needs to be tracked. In winter, signals at m/z 208 and 210 were found to only originate from $ClNO_2$, based on their correlation and the isotope ratios, which ruled out the $I\cdot{}^{79}Br^-$ interference. In summer, no $ClNO_2\cdot I^-$ nor $I\cdot Br^-$ was found at m/z 208 or 210.

We had previously observed that high NO_2 (500 ppbv) can interfere with HO_2NO_2 detection using I^- with a high resolution time-of-flight CIMS.[44] For this reason, NO_2 (up to 86 ppbv) was added to the inlet to test for possible interferences to the

DOI: 10.1021/acs.est.6b05169
Environ. Sci. Technol. 2017, 51, 3355−3363

Table 2. Summary of the Time-Dependent Model

	species/parameters
constrained	T,[a] p,[b] O_3,[c] NO,[c] NO_2,[c] H_2O(v),[d] CO,[d] CH_4,[d] C_2H_6,[d] C_3H_8,[d] CH_2O,[d] $CH_3C(O)CH_3$,[d] j values,[e]
time dependent	HO_2NO_2,[f] N_2O_5,[f] HONO,[f] PAN[f]
steady state	OH, HO_2, CH_3O_2, $CH_3C(O)O_2$, NO_3

[a]Fixed to different values for each run. [b]Fixed to be 100 kPa. [c]Constrained by measurements. [d]Fixed concentrations: [H_2O(v)] = 8000 ppmv, [CO] = 100 ppbv, [CH_4] = 1.8 ppmv, [C_2H_6] = 1 ppbv, [C_3H_8] = 500 pptv, [CH_2O] = 1 ppbv, and [$CH_3C(O)CH_3$] = 2 ppbv. [e]Estimated using the NCAR TUV model (https://www2.acom.ucar.edu/modeling/tropospheric-ultraviolet-and-visible-tuv-radiation-model). [f]Initial concentrations for time-dependent species: $[HO_2NO_2]_0$ = 2 pptv, $[N_2O_5]_0$ = 50 pptv, $[HONO]_0$ = 1 ppbv, and $[PAN]_0$ = 1 ppbv.

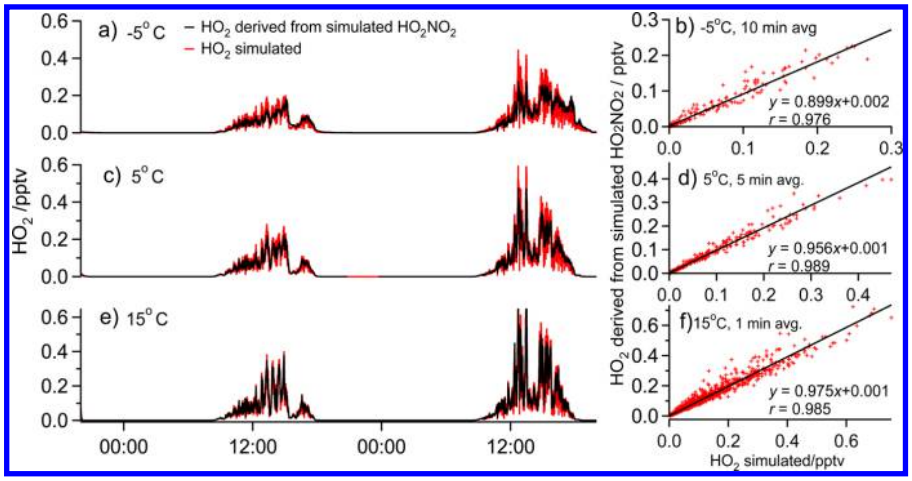

Figure 1. HO_2, HO_2NO_2, and HO_2 were simulated using the time-dependent model for a period of 24 h, with Δt = 10 s, at −5, 5, and 15 °C. (a, c, e) Time series of derived HO_2 from simulated HO_2NO_2 is plotted in red, and simulated HO_2 is plotted in black. (b, d, f) The derived and simulated HO_2 levels were averaged on different time scales and compared.

ambient measurement. However, no significant interferences due to NO_2 were found on either the $HO_2NO_2{\cdot}I^-$ or the NO_3^- channels.

A two-step indirect calibration was applied, as a portable HO_2NO_2 calibration source has not been developed. A known amount of Br_2 from a permeation tube (KIN-TEK) was periodically added into the inlet to track the sensitivity variation.[28,29]

$$Br_2 + I^-{\cdot}(H_2O)_n \rightarrow Br_2{\cdot}I^-(m/z\,285,\ 287,\ 289) + nH_2O \quad (9)$$

Br_2 is a convenient proxy as the CIMS instrument has similar sensitivities to HO_2NO_2 and Br_2 on the cluster channels. The Br_2 emission rate was determined every 2 or 3 days by a spectrophotometric method.[45,46] The relative sensitivity of HO_2NO_2 to Br_2 was determined in the laboratory by comparing signals of known amounts of HO_2NO_2 and Br_2. HO_2NO_2 was quantified by measuring the resulting NO_2 of HO_2NO_2 thermal decomposition with a cavity attenuated phase-shift spectroscopy[47] (CAPS, Aerodyne) (Supporting Information). The sensitivities to HO_2NO_2 ($HO_2NO_2{\cdot}I^-$ channel) were ∼25 and ∼15 Hz·pptv^{-1}, respectively, in both seasons. Commonly, we have estimated the limit of detection (LOD) based upon the standard deviation of the variations of background signals.[29,48] In this work, we defined the LOD as twice the standard deviation (2σ) of the background variation. The LODs of HO_2NO_2 for both seasons were 0.2 and 0.6 pptv, respectively, based on a 1 min integration time. The uncertainties for HO_2NO_2 measurement were 22% in winter and 16% in summer, mostly from calibration.

Determination of HO_2. HO_2NO_2 observations were combined with measurements of NO_2 and temperature to derive HO_2 levels from eq 5. HO_2NO_2 data were excluded during precipitation events, as they perturbed the equilibrium, or if they were below the LOD. All NO_2 data were well above the LOD. We applied different averaging times to derive HO_2 at different temperatures. Temperature ranged from −4.7 to 24.5 °C during the winter observation and 18.8 to 37.6 °C during the summer observation. The lifetime of HO_2NO_2 and thus the time scale to approach equilibrium varied. Also, NO_x emitted by traffic (especially traffic on the highway nearby) fluctuated, which can perturb the HO_2NO_2 equilibrium on short time scales.

We used a time-dependent model[21] to determine the appropriate averaging times. The model setup highlighted the influence of temperature and NO_x (Table 2). The chemical scheme is detailed in the Supporting Information. Model simulations were constrained to observed NO_x and O_3 from December 1, 2014, 20:00, to December 3, 2014, 20:00, when variations of NO_x were especially pronounced. Model simulations were performed for this period for a set of assumed temperatures. HO_2 was simulated directly from the model and also derived from model simulated HO_2NO_2 using eq 5. Both model simulated and experimentally derived HO_2 concentrations were averaged on different time scales and compared. The comparisons are shown in Figure 1. At −5 °C, 10 min averages of derived and simulated HO_2 agree within 10% (slope = 0.899, r = 0.976); at 5 °C, 5 min averages of derived and simulated HO_2 agree within 5% (slope = 0.955, r = 0.988); at 15 °C, 1 min averages of derived and simulated HO_2 agree within 3% (slope = 0.975, r = 0.985). Thus, we select the average time of 10 min for $-5\ °C \le T < 5\ °C$, 5 min for $5\ °C \le T < 15\ °C$, and 1 min for $T \ge 15\ °C$.

The uncertainty for HO_2 derived from HO_2NO_2 observations has multiple sources. The equilibrium constant K in eq 5 has a 30% uncertainty in the temperature range of our

DOI: 10.1021/acs.est.6b05169
Environ. Sci. Technol. 2017, 51, 3355−3363

Table 3. Species and Parameters for the Steady-State Model Prediction of HO_2

	species/parameters
constrained (measured)	T, p, O_3, H_2O(v), CO, NO, NO_2, HO_2NO_2,[a] N_2O_5,[b]
constrained (modeled/assumed)	j values,[c] CH_4[d], C_2H_6,[e] C_3H_8,[e] C_2H_4,[e] C_3H_6,[e] CH_2O,[e] CH_3OH[e], CH_3CHO,[e] PAN,[e] $CH_3C(O)CH_3$,[e] $CH_3C(O)CH_2OH$,[e] $CH_3C(O)CHO$,[e] isoprene,[e] $CH_3C(O)CH{=}CH_2$ (MVK),[e] $CH_2{=}C(CH_3)CHO$ (MACR),[e] benzene,[e] toluene,[e] HONO,[e] H_2O_2[e]
predicted by the model	OH, HO_2, CH_3O_2, $C_2H_5O_2$, $C_2H_4(OH)O_2$, $CH_3C(O)O_2$, $CH_3C(O)CH_2O_2$, Isop(OH)O_2,[f] $MOHO_2$,[g] MCO_3,[h] ArO_2,[i] $R(NO_3)O_2$,[j] NO_3, CH_3OOH

[a]Predicted by the steady-state model in Run_1; constrained by measurements in Run_2 (see text). [b]Constrained by measurement in the winter observation; estimated using the REAM model in the summer observation. [c]Estimated using the NCAR TUV model, scaled using the measured UV radiation. [d]CH_4 was fixed to be 1.8 ppmv. [e]Estimated using the REAM model. [f]Hydroxylperoxy radicals derived from the OH-initiated oxidation of isoprene. [g]Hydroxylperoxy radicals derived from the OH-initiated oxidations of MACR/MVK. [h]$CH_2{=}C(CH_3)C(O)O_2$. [i]Peroxy radicals derived from the oxidation of benzene and toluene. [j]Peroxyl radicals derived from the NO_3-alkene addition reactions.

observations[13,15,49,50] and is the major uncertainty source. The uncertainties of the HO_2NO_2 and NO_2 measurements are listed in Table 1. Combining these effects gives a total uncertainty of 39% in the winter observation and 35% in the summer observation for derived HO_2.

Model Calculation of HO_2. A steady-state model was used to estimate HO_2 to compare to HO_2 derived from observations. The model was developed on the basis of previous work in our laboratory.[20,21,51] The model setup is listed in Table 3. The chemistry scheme is listed in the Supporting Information. The model included detected species and meteorological parameters. VOC, HONO, and H_2O_2 were not measured. We estimated basic VOC (C_2H_6, C_3H_8, C_2H_4, C_3H_6, CH_2O, CH_3OH, CH_3CHO, peroxyacetyl nitrate (PAN), $CH_3C(O)CH_3$, $CH_3C(O)CH_2OH$, $CH_3C(O)CHO$, isoprene, methacrolein (MACR), methyl vinyl ketone (MVK), benzene, toluene), HONO, and H_2O_2 using the 3-D Regional chEmical and trAnsport Model (REAM). Details of REAM can be found in previous studies.[52−56] Average levels of key species given by REAM in both seasons are listed in Table 4. j values were calculated using the NCAR TUV model (https://www2.acom.ucar.edu/modeling/tropospheric-ultraviolet-and-visible-tuv-radiation-model) and scaled using measured solar UV radiation. The model was run twice. Run_1 was not constrained by measured HO_2NO_2 but calculated HO_2NO_2 to be in steady state. Run_2 included HO_2NO_2 as a constraint. Run_2 effectively makes HO_2NO_2 a HO_x source in the model and allows some compensation for sources that could be missing in the model.

Table 4. Average Concentrations of Key Species Predicted by REAM[a]

species	winter 2014	summer 2015
CH_2O	1.3	5.0
$CH_3C(O)CH_3$	2.1	2.3
HONO	0.76	0.30
toluene	0.83	0.41
isoprene	0.08	2.0

[a]unit: ppbv.

RESULTS AND DISCUSSION

Figures S7 and S8 show time series of HO_2NO_2, NO_2, NO, temperature, solar radiation, and derived HO_2. In winter, HO_2NO_2 ranged from the LOD to 21.1 pptv (average 3.7 pptv), NO_2 ranged from 2.7 to 60.1 ppbv (average 17.0 ppbv), and derived HO_2 was up to 3.5 pptv (daytime average 0.17 pptv). In summer, HO_2NO_2 ranged from the LOD to 90.3 pptv (average 11.7 pptv), NO_2 ranged from 1.4 to 64.6 ppbv (average 11.3 ppbv), and derived HO_2 was up to 89.3 pptv (daytime average 10.4 pptv). Figure 2 shows mean diurnal profiles of HO_2. Peak values of HO_2 profiles were 0.19 pptv in winter and 20.0 pptv in summer. These HO_2 levels are close to those observed in the same seasons at polluted sites.[6,57−59] In the following sections, we look at two test cases and model comparisons to determine if the derived HO_2 is reasonable.

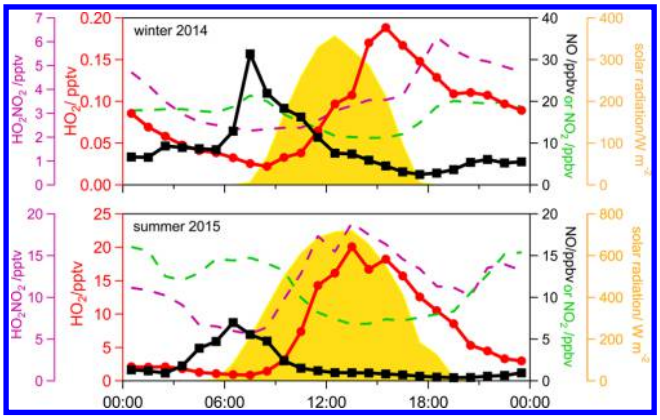

Figure 2. Diurnal profiles of derived HO_2, NO, and solar radiation in both winter and summer observations. NO suppressed HO_2 during morning rush hours. Diurnal profiles of HO_2NO_2 and NO_2 are also plotted in dotted lines.

Suppression of HO_2 at High NO. HO_2 can be efficiently suppressed at high NO due to the fast reaction of HO_2 with NO. The most obvious suppression of HO_2 occurred during morning rush hour, as seen in Figure 2. In both seasons, the peak of NO in the morning depressed HO_2, resulting in asymmetric diurnal profiles, although the radical production is expected to be symmetric as it follows the solar radiation. A similar behavior was observed in urban areas by Holland et al.[60] and Martinez et al.[57]

Low HO_2 associated with high NO was oftentimes observed in both seasons, during the day and night. Figure 3 displays two examples of the suppression of HO_2 at high NO peaks. On December 26 and 27, 2014, HO_2 decreased accordingly at high NO multiple times (20:00−23:00, 03:00−06:00, 07:40−08:30, 09:00−14:00). On June 20, 2015, HO_2 was around 1 pptv during 17:00−18:00 while NO was high up to 12 ppbv; then, HO_2 recovered to ∼6 pptv after NO dropped to ∼1 ppbv. In all, our derived HO_2 responded to NO accordingly. This indicates that there are no significant interferences when NO_x is high that lead to an obvious over estimation

DOI: 10.1021/acs.est.6b05169
Environ. Sci. Technol. 2017, 51, 3355−3363

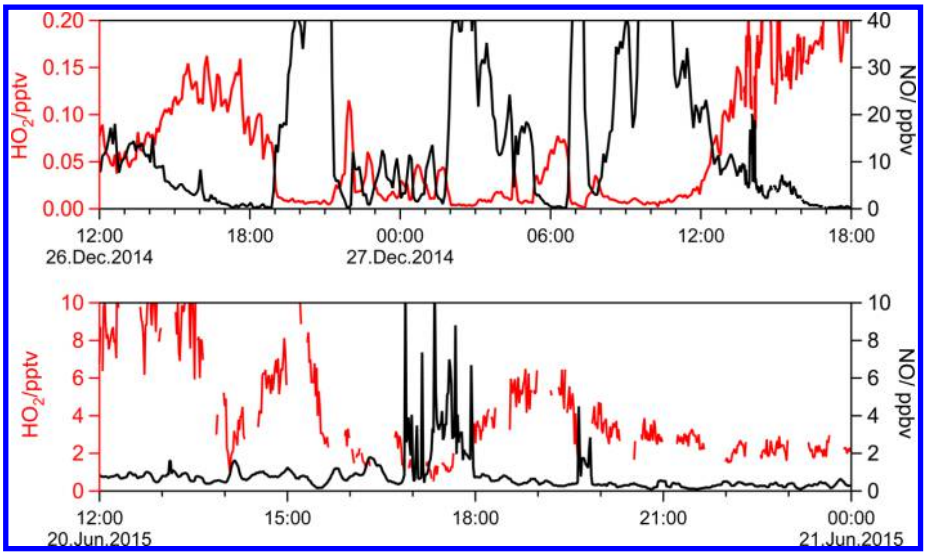

Figure 3. Examples of the suppression of HO_2 at high NO.

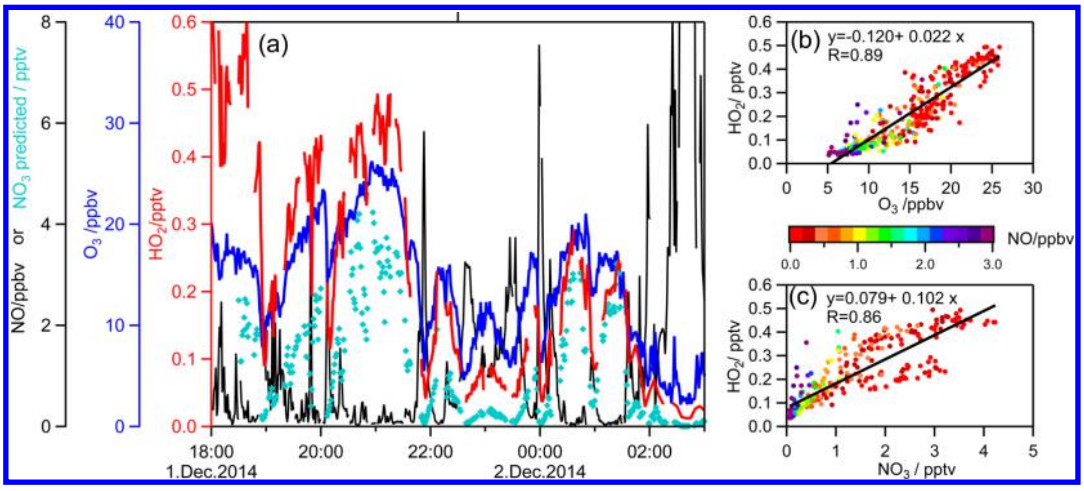

Figure 4. Correlation between HO_2 and O_3/NO_3 during 18:30−01:30 on the night of December 1 to 2, 2014.

of HO_2. However, very low levels of HO_2 were still observed at high NO.

Relationship between HO_2 and O_3/NO_3 at Night. Nighttime HO_x has been reported in several locations.[3,61] Nighttime HO_2 is largely produced by ozonolysis and oxidation of VOC by NO_3.[1,2,4,5,62−64] Here, we examine the correlation between nighttime HO_2 and O_3 in both seasons and the correlation between nighttime HO_2 and NO_3 in winter when N_2O_5 was measured, which allowed for an estimate of $[NO_3]$:

$$[NO_3] \approx \frac{k_{N_2O_5}[N_2O_5] + k_{NO_2+O_3}[NO_2][O_3]}{k_{NO_3+NO_2}[NO_2] + k_{NO_3+NO}[NO]} \quad (10)$$

where $k_{N_2O_5}$ is the unimolecular thermal decomposition rate of N_2O_5.

HO_2 was moderately correlated to O_3 at night for the both seasons. $r(HO_2-O_3)$ = 0.68 in the winter observation and 0.67 in summer. The correlation with NO_3 was found to be less, $r(HO_2-NO_3)$ = 0.27 in winter. However, if a filter of NO < 1 ppbv is applied, as high NO can suppress HO_2, O_3, and NO_3, then $r(HO_2-O_3)$ = 0.59 in winter and 0.47 in summer and $r(HO_2-NO_3)$ = 0.67 in winter.

Strong correlations between HO_2 and O_3/NO_3 were also observed on individual nights. For instance, as seen in Figure 4, during 18:30−01:30 on the night of December 1 to 2, 2014, most of the time NO < 1 ppbv, HO_2, O_3 and NO_3 all showed similar temporal patterns, $r(HO_2-O_3)$ = 0.89, and $r(HO_2-NO_3)$ = 0.86. Also, as seen in Figure 5, during 20:00−05:00 on the night of June 30 to July 1, 2015, NO was mostly <1 ppbv and $r(HO_2-O_3)$ = 0.90. These strong correlations suggest that O_3 and NO_3 were driving the production of HO_2 on these nights.

Comparison of Observation-Derived and Model-Predicted HO_2. Figure 6 compares the derived HO_2 with model predicted HO_2 (Run_1 and Run_2). (See Figures S7 and S8 for day-to-day variations of derived/model predicted HO_2 and other species.) As the model was not constrained by measured VOC, H_2O_2, HONO, and j values, discrepancies between model simulated and derived HO_2 are expected. Nevertheless, Run_1 still captures the features of HO_2. The average model-to-observed ratio (M/O) of Run_1 is 1.27 (r = 0.54) for winter and 0.70 (r = 0.80) for summer. For the summer observations, Run_1 tends to underestimate midday (e.g., June 15−18, 2015) and nighttime HO_2, which suggests that more sources of HO_2 may exist than are included in the model.

DOI: 10.1021/acs.est.6b05169
Environ. Sci. Technol. 2017, 51, 3355−3363

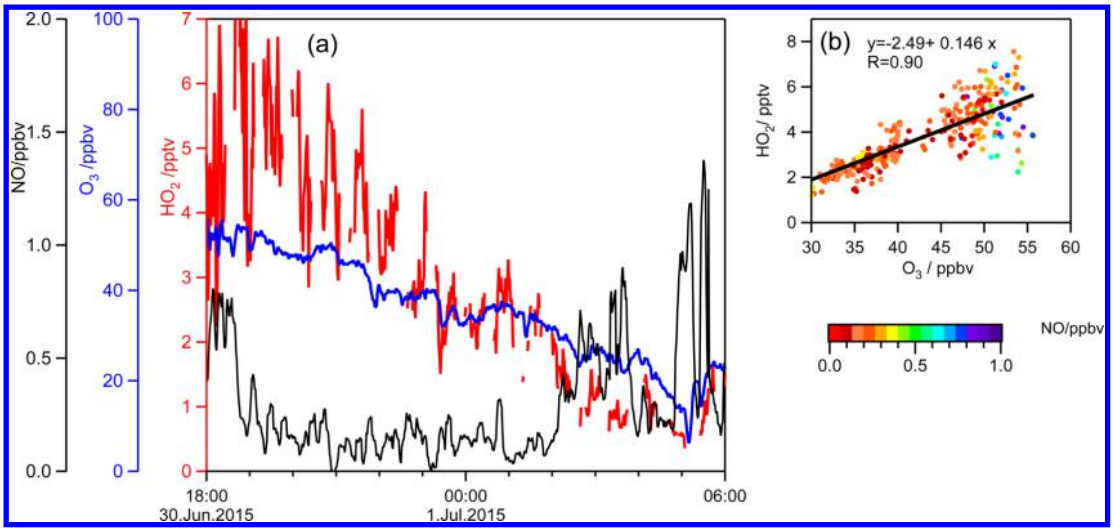

Figure 5. Correlation between HO_2 and O_3 during 20:00−05:00 on the night of June 30 to July 1, 2015.

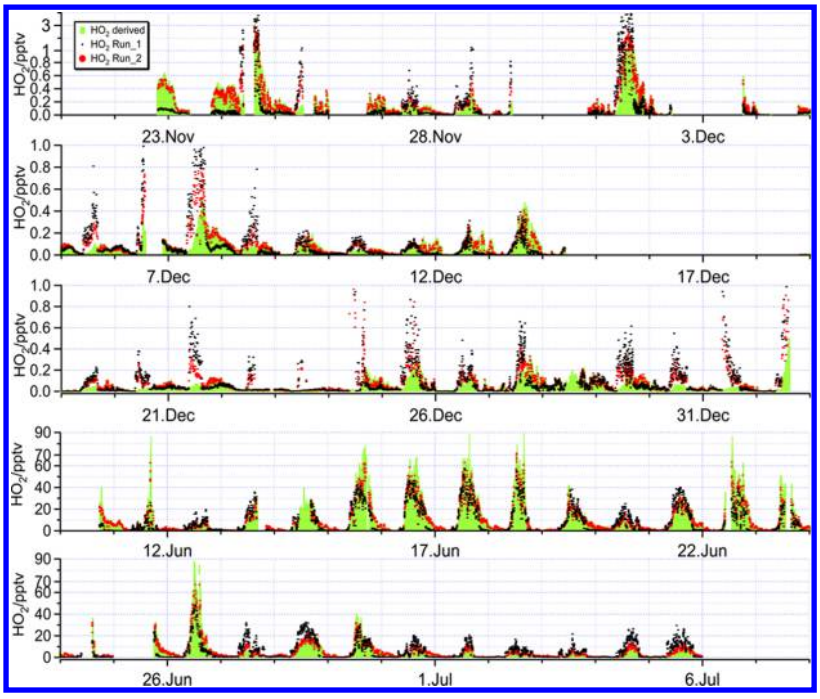

Figure 6. Comparison between the HO_2 derived from observations to that predicted by the steady-state model. Run_1 was not constrained by measured HO_2NO_2. Run_2 was constrained by measured HO_2NO_2. Note that scales are different in different seasons.

With the constraint of HO_2NO_2, Run_2 predicted HO_2 with average M/O = 1.13 (r = 0.77) for winter and average M/O = 0.90 (r = 0.97) for summer. Run_2 slightly improved M/O for the winter season and improved M/O for the summer season. Both model runs predicted peak midday HO_2 levels on several winter days, such as December 21−24, that were significantly higher than the observations. One likely explanation for this is the overprediction of HONO levels by the REAM model. HONO has heterogeneous sources,[65−67] which are difficult to parametrize. The photolysis of HONO becomes a more important source of HO_x in winter, as other sources such as the photolysis of ozone contribute less. As a result, predicted HONO has a larger impact on HO_2 prediction in winter. This also suggests the importance of better observational constraints in future studies. Nevertheless, considering the few observational constraints available, both model runs are in reasonable agreement with the derived HO_2.

Future Studies. Our study shows the feasibility of deriving HO_2 from HO_2NO_2 measurements in warm environments. Future work should focus on: (1) model calculation of HO_2 with a better constrained observational data set and (2) intercomparison with HO_2 measurement techniques such as laser-induced fluorescence (LIF).[68] In addition, a direct CIMS HO_2 measurement technique using Br^- as the reagent ion has recently been developed.[40] We plan on further comparisons with this method as well.

■ ASSOCIATED CONTENT

Supporting Information

The Supporting Information is available free of charge on the ACS Publications website at DOI: 10.1021/acs.est.6b05169.

Synthesis of HO_2NO_2; ion chemistry of HO_2NO_2 with $I^-\cdot(H_2O)_n$; calibration of HO_2NO_2; assessment of the

DOI: 10.1021/acs.est.6b05169
Environ. Sci. Technol. 2017, 51, 3355−3363

CIMS NO_3^- channel; chemistry scheme for the time-dependent and steady-state models; time series of observed HO_2NO_2, temperature, NO, NO_2, solar radiation, derived and model-predicted HO_2 (PDF)

AUTHOR INFORMATION

Corresponding Author

*E-mail: greg.huey@eas.gatech.edu; telephone: +1 (404) 894-5541 (L.G.H.).

ORCID

Dexian Chen: 0000-0001-6963-5205

Present Address

#D.C.: Center for Atmospheric Particle Studies, Carnegie Mellon University, Pittsburgh, Pennsylvania 15213, United States.

Notes

The authors declare no competing financial interest.

ACKNOWLEDGMENTS

This study was an extension of the studies of HO_2NO_2 at Summit, Greenland (NSF Grant #0908186) and during the DC3 campaign (NSF Grant #1063652). D.C., L.G.H., and D.J.T. were financially supported by NSF under both grants. N.L.N. was supported by NSF under grant #1455588. The meteorological data were provided by the Atlanta Midtown (Georgia Tech) Weather Station, colocated on top of the Ford ES&T building. We thank James R. Hite Jr. for processing the meteorological data. We also thank Dr. J. Michael Nicovich for synthesizing NO_2 and recalibrating our NO_2/N_2 standard.

REFERENCES

(1) Atkinson, R.; Carter, W. P. L. Kinetics and Mechanisms of the Gas-Phase Reactions of Ozone with Organic-Compounds under Atmospheric Conditions. *Chem. Rev.* **1984**, *84* (5), 437−470.

(2) Johnson, D.; Marston, G. The gas-phase ozonolysis of unsaturated volatile organic compounds in the troposphere. *Chem. Soc. Rev.* **2008**, *37*, 699−716.

(3) Geyer, A.; Bachmann, K.; Hofzumahaus, A.; Holland, F.; Konrad, S.; Klupfel, T.; Patz, H. W.; Perner, D.; Mihelcic, D.; Schafer, H. J.; Volz-Thomas, A.; Platt, U. Nighttime formation of peroxy and hydroxyl radicals during the BERLIOZ campaign: Observations and modeling studies. *J. Geophys. Res.* **2003**, *108* (D4), 8249.

(4) Paulson, S. E.; Orlando, J. J. The reactions of ozone with alkenes: An important source of HO_x in the boundary layer. *Geophys. Res. Lett.* **1996**, *23* (25), 3727−3730.

(5) Wayne, R. P.; Barnes, I.; Biggs, P.; Burrows, J. P.; Canosamas, C. E.; Hjorth, J.; Lebras, G.; Moortgat, G. K.; Perner, D.; Poulet, G.; Restelli, G.; Sidebottom, H. The nitrate radical - physics, chemistry, and the atmosphere. *Atmos. Environ., Part A* **1991**, *25* (1), 1−203.

(6) Kanaya, Y.; Cao, R. Q.; Akimoto, H.; Fukuda, M.; Komazaki, Y.; Yokouchi, Y.; Koike, M.; Tanimoto, H.; Takegawa, N.; Kondo, Y. Urban photochemistry in central Tokyo: 1. Observed and modeled OH and HO_2 radical concentrations during the winter and summer of 2004. *J. Geophys. Res.* **2007**, *112* (D21), D21312.

(7) Carlton, A. G.; Wiedinmyer, C.; Kroll, J. H. A review of Secondary Organic Aerosol (SOA) formation from isoprene. *Atmos. Chem. Phys.* **2009**, *9* (14), 4987−5005.

(8) Jenkin, M. E. Modelling the formation and composition of secondary organic aerosol from α- and β-pinene ozonolysis using MCM v3. *Atmos. Chem. Phys.* **2004**, *4*, 1741−1757.

(9) Finlayson-Pitts, B. J.; Pitts, J. N., Jr. *Chemistry of the upper and lower atmosphere: theory, experiments, and applications*; Academic Press: San Diego, USA, 2000.

(10) Jiménez, E.; Gierczak, T.; Stark, H.; Burkholder, J. B.; Ravishankara, A. R. Reaction of OH with HO_2NO_2 (peroxynitric acid): Rate coefficients between 218 and 335 K and product yields at 298 K. *J. Phys. Chem. A* **2004**, *108* (7), 1139−1149.

(11) Levine, S. Z.; Uselman, W. M.; Chan, W. H.; Calvert, J. G.; Shaw, J. H. Kinetics and mechanism of HO_2 + NO_2 reactions - significance of peroxynitric acid formation in photochemical smog. *Chem. Phys. Lett.* **1977**, *48* (3), 528−535.

(12) Niki, H.; Maker, P. D.; Savage, C. M.; Breitenbach, L. P. Fourier-transform IR spectroscopic observation of pernitric acid formed via HOO + NO_2 → $HOONO_2$. *Chem. Phys. Lett.* **1977**, *45* (3), 564−566.

(13) Gierczak, T.; Jiménez, E.; Riffault, V.; Burkholder, J. B.; Ravishankara, A. R. Thermal decomposition of HO_2NO_2 (peroxynitric acid, PNA): Rate coefficient and determination of the enthalpy of formation. *J. Phys. Chem. A* **2005**, *109* (4), 586−596.

(14) Slusher, D. L.; Huey, L. G.; Tanner, D. J.; Chen, G.; Davis, D. D.; Buhr, M.; Nowak, J. B.; Eisele, F. L.; Kosciuch, E.; Mauldin, R. L.; Lefer, B. L.; Shetter, R. E.; Dibb, J. E. Measurements of pernitric acid at the South Pole during ISCAT 2000. *Geophys. Res. Lett.* **2002**, *29* (21), 2011.

(15) Burkholder, J. B.; Sander, S. P.; Abbatt, J. P. D.; Barker, J. R.; Huie, R. E.; Kolb, C. E.; Kurylo, M. J.; Orkin, V. L.; Wilmouth, D. M.; Wine, P. H. *Chemical kinetics and photochemical data for use in atmospheric studies, evaluation No. 18*; Jet Propulsion Laboratory: Pasadena, USA, 2015.

(16) Talbot, R. W.; Dibb, J. E.; Scheuer, E. M.; Kondo, Y.; Koike, M.; Singh, H. B.; Salas, L. B.; Fukui, Y.; Ballenthin, J. O.; Meads, R. F.; Miller, T. M.; Hunton, D. E.; Viggiano, A. A.; Blake, D. R.; Blake, N. J.; Atlas, E.; Flocke, F.; Jacob, D. J.; Jaegle, L. Reactive nitrogen budget during the NASA SONEX mission. *Geophys. Res. Lett.* **1999**, *26* (20), 3057−3060.

(17) Jaeglé, L.; Jacob, D. J.; Brune, W. H.; Wennberg, P. O. Chemistry of HO_x radicals in the upper troposphere. *Atmos. Environ.* **2001**, *35* (3), 469−489.

(18) Chen, G.; Davis, D.; Crawford, J.; Hutterli, L. M.; Huey, L. G.; Slusher, D.; Mauldin, L.; Eisele, F.; Tanner, D.; Dibb, J.; Buhr, M.; McConnell, J.; Lefer, B.; Shetter, R.; Blake, D.; Song, C. H.; Lombardi, K.; Arnoldy, J. A reassessment of HO_x South Pole chemistry based on observations recorded during ISCAT 2000. *Atmos. Environ.* **2004**, *38* (32), 5451−5461.

(19) Chen, G.; Davis, D.; Crawford, J.; Nowak, J. B.; Eisele, F.; Mauldin, R. L.; Tanner, D.; Buhr, M.; Shetter, R.; Lefer, B.; Arimoto, R.; Hogan, A.; Blake, D. An investigation of South Pole HO_x chemistry: Comparison of model results with ISCAT observations. *Geophys. Res. Lett.* **2001**, *28* (19), 3633−3636.

(20) Sjostedt, S. Investigation of photochemistry at high lattitudes: comparison of model predictions to measurements of short lived species. Ph. D. Thesis, Georgia Institute of Technology, Atlanta, USA, 2006.

(21) Kim, S.; Huey, L. G.; Stickel, R. E.; Tanner, D. J.; Crawford, J. H.; Olson, J. R.; Chen, G.; Brune, W. H.; Ren, X.; Lesher, R.; Wooldridge, P. J.; Bertram, T. H.; Perring, A.; Cohen, R. C.; Lefer, B. L.; Shetter, R. E.; Avery, M.; Diskin, G.; Sokolik, I. Measurement of HO_2NO_2 in the free troposphere during the intercontinental chemical transport experiment - North America 2004. *J. Geophys. Res.* **2007**, *112* (D12), D12S01.

(22) Stiller, G. P.; von Clarmann, T.; Bruehl, C.; Fischer, H.; Funke, B.; Glatthor, N.; Grabowski, U.; Hopfner, M.; Jockel, P.; Kellmann, S.; Kiefer, M.; Linden, A.; Lopez-Puertas, M.; Tsidu, G. M.; Milz, M.; Steck, T.; Steil, B. Global distributions of HO_2NO_2 as observed by the Michelson Interferometer for Passive Atmospheric Sounding (MIPAS). *J. Geophys. Res.* **2007**, *112* (D9), D09314.

(23) Jones, A. E.; Brough, N.; Anderson, P. S.; Wolff, E. W. HO_2NO_2 and HNO_3 in the coastal Antarctic winter night: a "lab-in-the-field" experiment. *Atmos. Chem. Phys.* **2014**, *14* (21), 11843−11851.

(24) Spencer, K. M.; McCabe, D. C.; Crounse, J. D.; Olson, J. R.; Crawford, J. H.; Weinheimer, A. J.; Knapp, D. J.; Montzka, D. D.; Cantrell, C. A.; Hornbrook, R. S.; Mauldin, R. L.; Wennberg, P. O. Inferring ozone production in an urban atmosphere using measure-

DOI: 10.1021/acs.est.6b05169
Environ. Sci. Technol. 2017, 51, 3355−3363

ments of peroxynitric acid. *Atmos. Chem. Phys.* **2009**, *9* (11), 3697−3707.
(25) Zhang, R. Y.; Leu, M. T.; Keyser, L. F. Heterogeneous chemistry of HO_2NO_2 in liquid sulfuric acid. *J. Phys. Chem. A* **1997**, *101* (18), 3324−3330.
(26) Abida, O.; Mielke, L. H.; Osthoff, H. D. Observation of gas-phase peroxynitrous and peroxynitric acid during the photolysis of nitrate in acidified frozen solutions. *Chem. Phys. Lett.* **2011**, *511* (4−6), 187−192.
(27) Veres, P. R.; Roberts, J. M.; Wild, R. J.; Edwards, P. M.; Brown, S. S.; Bates, T. S.; Quinn, P. K.; Johnson, J. E.; Zamora, R. J.; de Gouw, J. Peroxynitric acid (HO_2NO_2) measurements during the UBWOS 2013 and 2014 studies using iodide ion chemical ionization mass spectrometry. *Atmos. Chem. Phys.* **2015**, *15* (14), 8101−8114.
(28) Neuman, J. A.; Nowak, J. B.; Huey, L. G.; Burkholder, J. B.; Dibb, J. E.; Holloway, J. S.; Liao, J.; Peischl, J.; Roberts, J. M.; Ryerson, T. B.; Scheuer, E.; Stark, H.; Stickel, R. E.; Tanner, D. J.; Weinheimer, A. Bromine measurements in ozone depleted air over the Arctic Ocean. *Atmos. Chem. Phys.* **2010**, *10* (14), 6503−6514.
(29) Liao, J.; Sihler, H.; Huey, L. G.; Neuman, J. A.; Tanner, D. J.; Friess, U.; Platt, U.; Flocke, F. M.; Orlando, J. J.; Shepson, P. B.; Beine, H. J.; Weinheimer, A. J.; Sjostedt, S. J.; Nowak, J. B.; Knapp, D. J.; Staebler, R. M.; Zheng, W.; Sander, R.; Hall, S. R.; Ullmann, K. A comparison of Arctic BrO measurements by chemical ionization mass spectrometry and long path-differential optical absorption spectroscopy. *J. Geophys. Res.* **2011**, *116* (D14), D00R02.
(30) Liao, J.; Huey, L. G.; Tanner, D. J.; Flocke, F. M.; Orlando, J. J.; Neuman, J. A.; Nowak, J. B.; Weinheimer, A. J.; Hall, S. R.; Smith, J. N.; Fried, A.; Staebler, R. M.; Wang, Y.; Koo, J. H.; Cantrell, C. A.; Weibring, P.; Walega, J.; Knapp, D. J.; Shepson, P. B.; Stephens, C. R. Observations of inorganic bromine (HOBr, BrO, and Br_2) speciation at Barrow, Alaska, in spring 2009. *J. Geophys Res-Atmos* **2012**, *117* (D14), D00R16.
(31) Liao, J.; Huey, L. G.; Liu, Z.; Tanner, D. J.; Cantrell, C. A.; Orlando, J. J.; Flocke, F. M.; Shepson, P. B.; Weinheimer, A. J.; Hall, S. R.; Ullmann, K.; Beine, H. J.; Wang, Y. H.; Ingall, E. D.; Stephens, C. R.; Hornbrook, R. S.; Apel, E. C.; Riemer, D.; Fried, A.; Mauldin, R. L.; Smith, J. N.; Staebler, R. M.; Neuman, J. A.; Nowak, J. B. High levels of molecular chlorine in the Arctic atmosphere. *Nat. Geosci.* **2014**, *7* (2), 91−94.
(32) Pratt, K. A.; Custard, K. D.; Shepson, P. B.; Douglas, T. A.; Pohler, D.; General, S.; Zielcke, J.; Simpson, W. R.; Platt, U.; Tanner, D. J.; Huey, L. G.; Carlsen, M.; Stirm, B. H. Photochemical production of molecular bromine in Arctic surface snowpacks. *Nat. Geosci.* **2013**, *6* (5), 351−356.
(33) Kercher, J. P.; Riedel, T. P.; Thornton, J. A. Chlorine activation by N_2O_5: simultaneous, in situ detection of $ClNO_2$ and N_2O_5 by chemical ionization mass spectrometry. *Atmos. Meas. Tech.* **2009**, *2* (1), 193−204.
(34) McNeill, V. F.; Patterson, J.; Wolfe, G. M.; Thornton, J. A. The effect of varying levels of surfactant on the reactive uptake of N_2O_5 to aqueous aerosol. *Atmos. Chem. Phys.* **2006**, *6*, 1635−1644.
(35) Le Breton, M.; McGillen, M. R.; Muller, J. B. A.; Bacak, A.; Shallcross, D. E.; Xiao, P.; Huey, L. G.; Tanner, D.; Coe, H.; Percival, C. J. Airborne observations of formic acid using a chemical ionization mass spectrometer. *Atmos. Meas. Tech.* **2012**, *5* (12), 3029−3039.
(36) Le Breton, M.; Bacak, A.; Muller, J. B. A.; Xiao, P.; Shallcross, B. M. A.; Batt, R.; Cooke, M. C.; Shallcross, D. E.; Bauguitte, S. J. B.; Percival, C. J. Simultaneous airborne nitric acid and formic acid measurements using a chemical ionization mass spectrometer around the UK: Analysis of primary and secondary production pathways. *Atmos. Environ.* **2014**, *83*, 166−175.
(37) Thornton, J. A.; Braban, C. F.; Abbatt, J. P. D. N_2O_5 hydrolysis on sub-micron organic aerosols: the effect of relative humidity, particle phase, and particle size. *Phys. Chem. Chem. Phys.* **2003**, *5* (20), 4593−4603.
(38) Woodward-Massey, R.; Taha, Y. M.; Moussa, S. G.; Osthoff, H. D. Comparison of negative-ion proton-transfer with iodide ion chemical ionization mass spectrometry for quantification of isocyanic acid in ambient air. *Atmos. Environ.* **2014**, *98*, 693−703.
(39) Phillips, G. J.; Pouvesle, N.; Thieser, J.; Schuster, G.; Axinte, R.; Fischer, H.; Williams, J.; Lelieveld, J.; Crowley, J. N. Peroxyacetyl nitrate (PAN) and peroxyacetic acid (PAA) measurements by iodide chemical ionisation mass spectrometry: first analysis of results in the boreal forest and implications for the measurement of PAN fluxes. *Atmos. Chem. Phys.* **2013**, *13* (3), 1129−1139.
(40) Sanchez, J.; Tanner, D. J.; Chen, D.; Huey, L. G.; Ng, N. L. A new technique for the direct detection of HO_2 radicals using bromide chemical ionization mass spectrometry (Br-CIMS): initial characterization. *Atmos. Meas. Tech.* **2016**, *9*, 3851−3861.
(41) Huey, L. G. Measurement of trace atmospheric species by chemical ionization mass spectrometry: Speciation of reactive nitrogen and future directions. *Mass Spectrom. Rev.* **2007**, *26* (2), 166−184.
(42) Hanson, D. R.; Ravishankara, A. R. The Reaction Probabilities of $ClONO_2$ and N_2O_5 on Polar Stratospheric Cloud Materials. *J. Geophys. Res.* **1991**, *96* (D3), 5081−5090.
(43) Slusher, D. L.; Huey, L. G.; Tanner, D. J.; Flocke, F. M.; Roberts, J. M. A thermal dissociation-chemical ionization mass spectrometry (TD-CIMS) technique for the simultaneous measurement of peroxyacyl nitrates and dinitrogen pentoxide. *J. Geophys. Res.* **2004**, *109* (D19), D19315.
(44) Sanchez, J. School of Chemical and Biochemical Engineering, Georgia Institute of Technology, Atlanta, GA, USA, personal communication, 2016.
(45) Wu, C.; Birky, M. M.; Hepler, L. G. Thermochemistry of some bromine and iodine species in aqueous solution. *J. Phys. Chem.* **1963**, *67* (6), 1202−1205.
(46) Kazantseva, N. N.; Ernepesova, A.; Khodjamamedov, A.; Geldyev, O. A.; Krumgalz, B. S. Spectrophotometric analysis of iodide oxidation by chlorine in highly mineralized solutions. *Anal. Chim. Acta* **2002**, *456* (1), 105−119.
(47) Kebabian, P. L.; Wood, E. C.; Herndon, S. C.; Freedman, A. A practical alternative to chemiluminescence-based detection of nitrogen dioxide: Cavity attenuated phase shift spectroscopy. *Environ. Sci. Technol.* **2008**, *42* (16), 6040−6045.
(48) Neuman, J. A.; Huey, L. G.; Dissly, R. W.; Fehsenfeld, F. C.; Flocke, F.; Holecek, J. C.; Holloway, J. S.; Hubler, G.; Jakoubek, R.; Nicks, D. K.; Parrish, D. D.; Ryerson, T. B.; Sueper, D. T.; Weinheimer, A. J. Fast-response airborne in situ measurements of HNO_3 during the Texas 2000 Air Quality Study. *J. Geophys. Res.* **2002**, *107* (D20), 4436.
(49) Christensen, L. E.; Okumura, M.; Sander, S. P.; Friedl, R. R.; Miller, C. E.; Sloan, J. J. Measurements of the rate constant of $HO_2+NO_2+N_2 \rightarrow HO_2NO_2+N_2$ using near-infrared wavelength-modulation spectroscopy and UV-visible absorption spectroscopy. *J. Phys. Chem. A* **2004**, *108* (1), 80−91.
(50) Bacak, A.; Cooke, M. C.; Bardwell, M. W.; McGillen, M. R.; Archibald, A. T.; Huey, L. G.; Tanner, D.; Utembe, S. R.; Jenkin, M. E.; Derwent, R. G.; Shallcross, D. E.; Percival, C. J. Kinetics of the HO_2 + NO_2 Reaction: On the impact of new gas-phase kinetic data for the formation of HO_2NO_2 on HO_x, NO_x and HO_2NO_2 levels in the troposphere. *Atmos. Environ.* **2011**, *45* (35), 6414−6422.
(51) Liao, J.; Huey, L. G.; Tanner, D. J.; Brough, N.; Brooks, S.; Dibb, J. E.; Stutz, J.; Thomas, J. L.; Lefer, B.; Haman, C.; Gorham, K. Observations of hydroxyl and peroxy radicals and the impact of BrO at Summit, Greenland in 2007 and 2008. *Atmos. Chem. Phys.* **2011**, *11* (16), 8577−8591.
(52) Choi, Y.; Wang, Y. H.; Zeng, T.; Martin, R. V.; Kurosu, T. P.; Chance, K. Evidence of lightning NO_x and convective transport of pollutants in satellite observations over North America. *Geophys. Res. Lett.* **2005**, *32* (2), L02805.
(53) Jing, P.; Cunnold, D.; Choi, Y.; Wang, Y. Summertime tropospheric ozone columns from Aura OMI/MLS measurements versus regional model results over the United States. *Geophys. Res. Lett.* **2006**, *33* (17), L17817.

DOI: 10.1021/acs.est.6b05169
Environ. Sci. Technol. 2017, 51, 3355−3363

(54) Wang, Y. H.; Choi, Y. S.; Zeng, T.; Ridley, B.; Blake, N.; Blake, D.; Flocke, F. Late-spring increase of trans-Pacific pollution transport in the upper troposphere. *Geophys. Res. Lett.* **2006**, *33* (1), L01811.
(55) Liu, Z.; Wang, Y. H.; Gu, D. S.; Zhao, C.; Huey, L. G.; Stickel, R.; Liao, J.; Shao, M.; Zhu, T.; Zeng, L. M.; Liu, S. C.; Chang, C. C.; Amoroso, A.; Costabile, F. Evidence of reactive aromatics as a major source of peroxy acetyl nitrate over China. *Environ. Sci. Technol.* **2010**, *44* (18), 7017−7022.
(56) Zhao, C.; Wang, Y. H.; Yang, Q.; Fu, R.; Cunnold, D.; Choi, Y. Impact of East Asian summer monsoon on the air quality over China: View from space. *J. Geophys. Res.* **2010**, *115*, D09301.
(57) Martinez, M.; Harder, H.; Kovacs, T. A.; Simpas, J. B.; Bassis, J.; Lesher, R.; Brune, W. H.; Frost, G. J.; Williams, E. J.; Stroud, C. A.; Jobson, B. T.; Roberts, J. M.; Hall, S. R.; Shetter, R. E.; Wert, B.; Fried, A.; Alicke, B.; Stutz, J.; Young, V. L.; White, A. B.; Zamora, R. J. OH and HO_2 concentrations, sources, and loss rates during the Southern Oxidants Study in Nashville, Tennessee, summer 1999. *J. Geophys Res-Atmos* **2003**, *108* (D19), 4617.
(58) Ren, X. R.; Brune, W. H.; Mao, J. Q.; Mitchell, M. J.; Lesher, R. L.; Simpas, J. B.; Metcalf, A. R.; Schwab, J. J.; Cai, C. X.; Li, Y. Q.; Demerjian, K. L.; Felton, H. D.; Boynton, G.; Adams, A.; Perry, J.; He, Y.; Zhou, X. L.; Hou, J. Behavior of OH and HO_2 in the winter atmosphere in New York city. *Atmos. Environ.* **2006**, *40*, S252−S263.
(59) Shirley, T. R.; Brune, W. H.; Ren, X.; Mao, J.; Lesher, R.; Cardenas, B.; Volkamer, R.; Molina, L. T.; Molina, M. J.; Lamb, B.; Velasco, E.; Jobson, T.; Alexander, M. Atmospheric oxidation in the Mexico City Metropolitan Area (MCMA) during April 2003. *Atmos. Chem. Phys.* **2006**, *6*, 2753−2765.
(60) Holland, F.; Hofzumahaus, A.; Schafer, R.; Kraus, A.; Patz, H. W. Measurements of OH and HO_2 radical concentrations and photolysis frequencies during BERLIOZ. *J. Geophys. Res.* **2003**, *108* (D4), 8246.
(61) Commane, R.; Floquet, C. F. A.; Ingham, T.; Stone, D.; Evans, M. J.; Heard, D. E. Observations of OH and HO_2 radicals over West Africa. *Atmos. Chem. Phys.* **2010**, *10* (18), 8783−8801.
(62) Brown, S. S.; de Gouw, J. A.; Warneke, C.; Ryerson, T. B.; Dube, W. P.; Atlas, E.; Weber, R. J.; Peltier, R. E.; Neuman, J. A.; Roberts, J. M.; Swanson, A.; Flocke, F.; McKeen, S. A.; Brioude, J.; Sommariva, R.; Trainer, M.; Fehsenfeld, F. C.; Ravishankara, A. R. Nocturnal isoprene oxidation over the Northeast United States in summer and its impact on reactive nitrogen partitioning and secondary organic aerosol. *Atmos. Chem. Phys.* **2009**, *9* (9), 3027−3042.
(63) Sommariva, R.; Osthoff, H. D.; Brown, S. S.; Bates, T. S.; Baynard, T.; Coffman, D.; de Gouw, J. A.; Goldan, P. D.; Kuster, W. C.; Lerner, B. M.; Stark, H.; Warneke, C.; Williams, E. J.; Fehsenfeld, F. C.; Ravishankara, A. R.; Trainer, M. Radicals in the marine boundary layer during NEAQS 2004: a model study of day-time and night-time sources and sinks. *Atmos. Chem. Phys.* **2009**, *9* (9), 3075−3093.
(64) Sommariva, R.; Brown, S. S.; Roberts, J. M.; Brookes, D. M.; Parker, A. E.; Monks, P. S.; Bates, T. S.; Bon, D.; de Gouw, J. A.; Frost, G. J.; Gilman, J. B.; Goldan, P. D.; Herndon, S. C.; Kuster, W. C.; Lerner, B. M.; Osthoff, H. D.; Tucker, S. C.; Warneke, C.; Williams, E. J.; Zahniser, M. S. Ozone production in remote oceanic and industrial areas derived from ship based measurements of peroxy radicals during TexAQS 2006. *Atmos. Chem. Phys.* **2011**, *11* (6), 2471−2485.
(65) Zhou, X. L.; Gao, H. L.; He, Y.; Huang, G.; Bertman, S. B.; Civerolo, K.; Schwab, J. Nitric acid photolysis on surfaces in low-NO_x environments: Significant atmospheric implications. *Geophys. Res. Lett.* **2003**, *30* (23), 2217.
(66) Wang, S. H.; Ackermann, R.; Spicer, C. W.; Fast, J. D.; Schmeling, M.; Stutz, J. Atmospheric observations of enhanced NO_2 -HONO conversion on mineral dust particles. *Geophys. Res. Lett.* **2003**, *30* (11), 1595.
(67) Liu, Z.; Wang, Y. H.; Costabile, F.; Amoroso, A.; Zhao, C.; Huey, L. G.; Stickel, R.; Liao, J.; Zhu, T. Evidence of aerosols as a media for rapid daytime HONO production over China. *Environ. Sci. Technol.* **2014**, *48* (24), 14386−14391.
(68) Fuchs, H.; Holland, F.; Hofzumahaus, A. Measurement of tropospheric RO_2 and HO_2 radicals by a laser-induced fluorescence instrument. *Rev. Sci. Instrum.* **2008**, *79* (8), 084104.
(69) Ryerson, T. B.; Williams, E. J.; Fehsenfeld, F. C. An efficient photolysis system for fast-response NO_2 measurements. *J. Geophys Res-Atmos* **2000**, *105* (D21), 26447−26461.

DOI: 10.1021/acs.est.6b05169
Environ. Sci. Technol. 2017, 51, 3355−3363